JOURNAL OF MATERIALS SCIENCE **39** (2004) 4861–4868

Cesium immobilization into an apatitic structure

L. CAMPAYO, F. AUDUBERT*, J. E. LARTIGUE
CEA Cadarache, DEN/DED/SEP/LCC, 13108 Saint Paul Lez Durance, France
E-mail: fabienne.audubert@cea.fr

D. BERNACHE-ASSOLLANT
SPCTS, Université de Limoges, 123 av. Albert Thomas, 87060 Limoges Cedex, France
E-mail: bernache@unilim.fr

Apatitic structure has been investigated as a potential host matrix for cesium issued from high level nuclear wastes. The aqueous behavior of such a substituted silicate compound revealed poor properties to retain this element. They were mainly due to the presence of Cs-bearing quickly soluble phases. Attempts to synthesize materials with different composition or cesium content showed that this element was still distributed between several phases. Particularly, in the case of calcium compounds, a new phosphate, $CaCsNd(PO_4)_2$, was usually formed when cesium was added and remained in the system after being exposed to a leach test procedure. © *2004 Kluwer Academic Publishers*

1. Introduction

During the reprocessing of spent nuclear fuel, high level wastes containing fission products are generated. Because of their toxicity over several decades, these wastes have focused the attention of governments as well as public opinion. De facto, some radionuclides, like ^{129}I and ^{135}Cs, exhibit a radioactive half-life greater than one million years [1] and could remain harmful even after their conditioning and disposal into a geological repository.

In case of a groundwater contamination, iodine and cesium are believed to be the first radionuclides to reach the biosphere due to their high mobility [2]. That is why, they have to be efficiently immobilized. Therefore, the study of natural minerals at the fossil nuclear reactor of Oklo (Gabon) gave information of great importance about the structures able to retain these radionuclides [3]. Crystalline phases with apatitic structure have proven to be in this way interesting candidates [4].

A general formula for apatites could be written as $Me_{10}(XO_4)_6Z_2$ (Me = Ca, Sr, ...; X = P, V, ...; Z = F, Cl, ...). If their inner ability to restore their lattice at low temperature after being exposed to an irradiation damage [5] was the origin of their investigation in the nuclear field, apatites also have other interesting properties. Specifically, they are highly stable in neutral to alkaline pH [6]. This point could be therefore considered as advantageous for their durability in geological environments. Within the apatite family, fluorine substituted ones appear to be the less soluble and those with the highest thermal resistance [7].

Many works deal with the incorporation of stable isotopes of fission products into apatites. For example, iodine confinement was established in such a structure of formula $Pb_{10}(VO_4)_{4,8}(PO_4)_{1,2}I_2$ [8–11] and trivalent cations, like earth elements, were successfully immobilized in a pure $Ca_9Nd(PO_4)_5(SiO_4)F_2$ phase [12, 13]. The introduction of a trivalent cation like neodymium then required the replacement of a trivalent phosphate group by a tetravalent silicate. These silicate substituted apatites are called britholites. Apatitic structure also seems to be able to incorporate monovalent cations like alkaline elements [14–16]. Nevertheless, a little was found about cesium specific incorporation.

Literature survey points out that cesium could be immobilized in a $Ca_7Nd_2Cs(PO_4)_5(SiO_4)FO_{0.5}$-type phase [17, 18]. That is why this particular composition with different cesium amounts (10 and 4 wt%) was investigated and an extrapolation to a barium apatite was performed (this latter composition taking into account ^{135}Cs disintegration into ^{135}Ba).

2. Materials and methods

2.1. Materials

The different powders were synthesized via conventional ceramic route, viz., the solid-state reaction. $CaCO_3$ (99%, Rectapur, Prolabo, France), SiO_2 (99%, Prolabo, France), Nd_2O_3 (99%, Merck, Germany), CaF_2 (98%, Rectapur, Prolabo, France), $BaCO_3$ (99.5%, Normapur, Prolabo, France), BaF_2 (98%, Normapur, Prolabo, France), $(NH_4)_2HPO_4$ (99%, Normapur, Prolabo, France), $Ba(NO_3)_2$ (99%, Merck, Germany), tri-calcium phosphate (Rectapur, Prolabo, France), $CaHPO_4$, $2H_2O$ (98%, Fluka Chemika, Switzerland) and Cs_2CO_3 (98%, Rectapur, Prolabo, France) were used as starting materials. Before weighing, Nd_2O_3 was annealed at 1000°C for 3 h to decompose $Nd(OH)_3$ traces. In the same way, Cs_2CO_3, which

*Author to whom all correspondence should be addressed.

TABLE I Chemical formula of Cs-bearing apatites and stoichiometric coefficients of Equations 1 and 2 for different cesium concentrations

Cs bearing apatite formula	a	b	c	d	e	f
1—$Ca_7Nd_2Cs(PO_4)_5SiO_4FO_{0.5}$	2.5	1.5	1	1	0.5	0.5
2—$Ca_{8.1}Nd_{1.54}Cs_{0.36}(PO_4)_5SiO_4F_{1.82}O_{0.18}$	2.5	2.19	1	0.77	0.91	0.18
3—$Ca_8NdCs(PO_4)_6FO_{0.5}$	3	1.5	0	0.5	0.5	0.5
4—$Ca_{9.18}Nd_{0.49}Cs_{0.32}(PO_4)_6F_{1.84}O_{0.16}$	3	2.26	0	0.245	0.92	0.16

is a highly hygroscopic compound, was annealed at 300°C for 1 h to remove adsorbed water.

$Ca_2P_2O_7$ was obtained from $CaHPO_4$, $2H_2O$ dehydration performed at 1000°C for 3 h:

$$2CaHPO_4, 2H_2O \rightarrow Ca_2P_2O_7 + 3H_2O$$

$Ba_2P_2O_7$ was obtained in the same way from the dehydration of $BaHPO_4$ (water precipitated from $Ba(NO_3)_2$ and $(NH_4)_2HPO_4$).

The synthesis route was in two steps. Firstly, the annealing of all the required elements, except cesium, in order to carry out a primary reaction to form an intermediate precursor. Secondly, cesium carbonate was added to that precursor and both were annealed in such a way that cesium volatilization could be prevented. In fact, as cesium carbonate is decomposed above 800°C with cesium loss, the annealing temperature for the second step was limited to 800°C. Equations 1 and 2 are representative of the overall process and Table I gives the values of the different stoichiometric coefficients depending on the cesium concentration and the apatitic composition. The barium apatite $Ba_8NdCs(PO_4)_6FO_{0.5}$ was synthesized similarly to the calcium apatite "3" in Table I.

Equation 1, step 1 (intermediate precursor synthesis):

$$aCa_2P_2O_7 + bCaCO_3 + cSiO_2 + dNd_2O_3 + eCaF_2 \rightarrow \text{“}Ca_xNd_y\square_{(10-x-y)}(PO_4)_z(SiO_4)_{(6-z)}F_{2e}o_{(2-2e)}\text{”} + bCO_2$$

Equation 2, step 2 (Cs-bearing apatite, synthesis)

$$\text{“}Ca_xNd_y\square_{(10-x-y)}(PO_4)_z(SiO_4)_{(6-z)}F_{2e}\square_{(2-2e)}\text{”} + fCs_2CO_3 \rightarrow Ca_xNd_yCs_{(10-x-y)}(PO_4)_z \times (SiO_4)_{(6-z)}F_{2e}O_f\square_{(2-2e-t)} + fCO_2$$

"□" stands for a vacancy and "$Ca_xNd_y\square_{(10-x-y)}(PO_4)_z(SiO_4)_{(6-z)}F_{2e}\square_{(2-2e)}$" for the expected precursor. "*e*" and "*t*" values are set by those of "*x*", "*y*" and "*z*". It should also be noted that the real precursor is a framework of several phases (see Section 3.1). For a better understanding we have chosen to change its writing into the equivalent formula of a cationic-deficient apatite surrounded by a **“ ”** symbol. In the same way, in order to make the reading of tables easier, vacancies are not marked. This convention is applied in the remaining part of this document.

2.2. Characterizations

The crystalline phases obtained were identified using a Brüker AXS D8 Advance diffractometer (λ_{Cu} = 1.5406 Å). The diffractograms were compared to the ICDD base data. When different phases were observed, their relative amounts were qualitatively determined by comparing the intensity of their main reflections.

Thermogravimetric and differentialthermo analysis (TGA-DTA) were performed on a Setaram TG-DTA 92-16.18 analyzer. A sample of 50 mg was introduced in a platinum crucible and then heated at a rate of 5 or 10°C/min. The carrier gas used was air.

Sintering was carried out on a pellet of 10 mm in diameter, pressed under 100 MPa, using a Setaram TMA 92–16.18 analyzer. Specific surface area was deduced from the measurement of the BET surface on a Micromeritics GEMINI 2360 with nitrogen as adsorbing gas. Bulk density of the sintered pellet was obtained through a geometric measurement and further determined on a Micromeritics ACCUPYC 1330 He-pycnometer.

Samples were carbon coated before being observed by scanning electron microscopy (SEM). Images were acquired on a Philips XL30 equipped with an Oxford Instruments EDX Isis analyzer. Because of poor assessment of fluorine amounts due to this technique, this amount has been arbitrarily set to 0.75 atoms per unit cell in the calculation of the apatite formula. The other elements were calculated from an algorithm based on the presence of 40 atoms per cell (42 minus 2 fluorine) with a filling of channels by oxygens to respect electric neutrality. For phases other than apatite, conventional calculation from the software was used. Non-sintered materials were inserted into a resin before polishing and coating.

Chemical analyzes were performed at the Bureau de Recherches Géologiques et Minières (Orléans, France). Neodymium was measured out by inductively coupled plasma mass spectrometry (ICP/MS), calcium and cesium by inductively coupled plasma optical emission spectroscopy (ICP/OES), phosphorus and silicon by atomic absorption spectroscopy (AAS) and fluorine by ionic chromatography.

Leaching experiment was performed at 100°C using a stainless steel soxhlet extractor apparatus where the leaching solution was distilled water. The test was run over 30 days. An overview of this procedure is more precisely described in [19]. Leachates were analyzed by AAS for cesium and calcium, by ionic chromatography for fluorine and by ICP/MS for neodymium and phosphorus. Only cesium data will be presented in this document.

TABLE II Operating data for the precursor synthesis

Precursor	ΔM_{th} (%)	ΔM_{exp} (%)	T_{min} (°C)	T_{max} (°C)	$T_{Annealing}$ (°C)
1 "$Ca_7Nd_2(PO_4)_5SiO_4F$"	5.41	5.34	860	1500	1400
2 "$Ca_{8.10}Nd_{1.54}(PO_4)_5SiO_4F_{1.82}$"	7.74	8.22	920	1250	1200
3 "$Ca_8Nd(PO_4)_6F$" (*)	5.89	n.p.	n.p.	n.p.	1400
4 "$Ca_{9.18}Nd_{0.49}(PO_4)_6F_{1.84}$"	8.69	8.27	860	1250	1200
5 "$Ba_8Nd(PO_4)_6F$"	3.48	3.68	950	1300	1200

ΔM_{th}, expected weight loss; ΔM_{exp}, observed weight loss; T_{min}, lower limit; T_{max}, upper limit; $T_{Annealing}$, synthesis temperature; (*) from: [18]; n.p.: non precised.

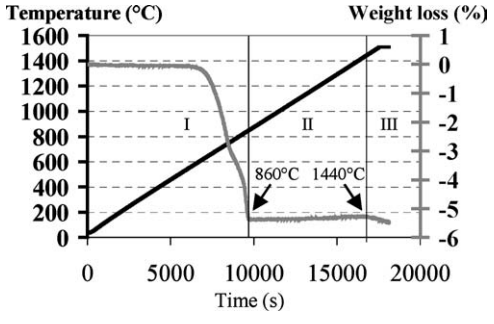

Figure 1 TGA of "$Ca_7Nd_2(PO_4)_5SiO_4F$" synthesis: I, gas release; II, annealing zone; III, decomposition.

3. Results and discussion

3.1. Synthesis of intermediate precursors

The reactions (Equation 1) were followed by thermogravimetric analysis (TGA) to set the lower and the upper annealing temperature to be used (Fig. 1). These values were determined from the comparison between observed and expected weight loss: a lower loss being inadequate for a complete reaction and a higher loss being indicative of a volatilization phenomenon. Expected weight loss was deduced from the theoretical Equation 1. Table II summarizes these results and the operating data finally exploited.

Because of cesium volatilization during Cs_2CO_3 melting above 800°C, the reaction between the intermediate precursor and Cs_2CO_3 should occur for a temperature lower than 800°C. Therefore, a thermal stability of the intermediate precursor up to 800°C was required. Table II shows that this prerequisite is verified and that no significant difference between observed and expected weight loss was noted. Annealing times for the precursors syntheses were then arbitrarily set to 6 h.

Annealed powders after cooling were characterized by X-ray diffraction. All the materials obtained were found to be composed of several phases. It is worth noting that silica was not expected to be detected by this technique as it was mainly amorphous. The equivalent cationic deficient apatite given previously as a writing convenience was never observed (Table III).

Moreover, the composition of the precursor changed with the annealing temperature. This point was illustrated in the case of "$Ca_7Nd_2(PO_4)_5(SiO_4)F$": Table IV shows the identification of the different phases as a function of annealing conditions.

Finally, the reactivity toward cesium carbonate could be expected to greatly depend on annealing conditions of the precursor. This point will be discussed later.

TABLE III Phases identification of the synthesized precursors

Precursor	Phases detected by means of X-ray diffraction
1 "$Ca_7Nd_2(PO_4)_5(SiO_4)F$"	$Ca_9Nd(PO_4)_5(SiO_4)F_2$ (M), $NdPO_4$ (M), $Ca_3(PO_4)_2$ (M).
2 "$Ca_{8.10}Nd_{1.54}(PO_4)_5(SiO_4)F_{1.82}$"	$Ca_{10}(PO_4)_6F_2$ (M), $Nd_3(PO_4)O_3$ (M), Nd_2O_3 (M), $NdPO_4$ (m).
3 "$Ca_8Nd(PO_4)_6F$"	$Ca_{10}(PO_4)_6F_2$ (M), $Ca_3(PO_4)_2$ (M), $NdPO_4$ (m).
4 "$Ca_{9.18}Nd_{0.49}(PO_4)_6F_{1.84}$"	$Ca_{10}(PO_4)_6F_2$ (M), $Ca_3(PO_4)_2$ (m), $NdPO_4$ (m).
5 "$Ba_8Nd(PO_4)_6F$"	$Ca_{10}(PO_4)_6F_2$ (M), $Ba_3(PO_4)_2$ (M), $Ba_3Nd(PO_4)_3$ (M).

M: major; m: minor; PDF 09-0169 and 45-0346 were found to explain the indexation of a same group of reflections. They corresponded to the theoretical formula $Ca_3(PO_4)_2$ and $Ca_9Nd(PO_4)_7$ respectively. To make easier the reading of the following tables, we arbitrarily decided to only make appear the first writing. This choice do not presume of the possible presence of the second phase.

TABLE IV Phases identification for the synthesis of "$Ca_7Nd_2(PO_4)_5(SiO_4)F$" as a function of annealing conditions

Annealing conditions	Phases detected by means of X-ray diffraction
800°C-6 h	Nd_2O_3 (M), $Ca_2P_2O_7$ (m), CaF_2 (m), CaO (m), $Ca_{10}(PO_4)_6F_2$ (t).
1000°C-6 h	$Ca_{10}(PO_4)_6F_2$ (M), Nd_2O_3 (M), $NdPO_4$ (M), $Nd_3(PO_4)O_3$ (M), CaO (m).
1200°C-6 h	$Ca_{10}(PO_4)_6F_2$ (M), $NdPO_4$ (M), $Ca_3(PO_4)_2$ (t), $Nd_3(PO_4)O_3$ (m).
1400°C-6 h (*)	$Ca_9Nd(PO_4)_5(SiO_4)F_2$ (M), $NdPO_4$ (M), $Ca_3(PO_4)_2$ (M).
1500°C-6 h	$Ca_9Nd(PO_4)_5(SiO_4)F_2$ (M), $Ca_3(PO_4)_2$ (M).

M: major; m: minor; t: traces; (*): from [18].

3.2. Synthesis of the Cs-bearing calcium/barium apatite

Synthesis of the Cs-bearing calcium/barium apatite was followed by TGA. Equation 2 shows that the reaction between Cs_2CO_3 and the calcium/barium deficient apatite leads to a loss of carbon dioxide. This release was thus observed on the thermogravimetric curves and temperatures at which synthesis occurred were deduced (Fig. 2, Table V).

No significant difference between the expected and the observed weight loss was noted. In all cases, the reactions occurred below 800°C. Consequently, powders were annealed for 1 h at various temperatures within the reaction temperature range.

The chemical composition of the sample after annealing was determined by XRD analysis and is

TABLE V Operating data for the Cs-bearing apatites syntheses

Cs-bearing apatite	ΔM_{th} (%)	ΔM_{exp} (%)	T_{start} (°C)	T_{end} (°C)	$T_{Annealing}$ (°C)
1 $Ca_7Nd_2Cs(PO_4)_5(SiO_4)FO_{0.5}$	1.67	1.30	500	800	500
					700
					750
					800
					820 (*)
2 $Ca_{8.10}Nd_{1.54}Cs_{0.36}(PO_4)_5(SiO_4)F_{1.82}O_{0.18}$	0.66	0.56	530	760	500
					800
3 $Ca_8NdCs(PO_4)_6FO_{0.5}$	1.81	1.10 (*)	640 (*)	790 (*)	770 (*)
4 $Ca_{9.18}Nd_{0.49}Cs_{0.33}(PO_4)_6F_{1.84}O_{0.16}$	0.67	0.46	560	740	500
					800
5 $Ba_8NdCs(PO_4)_6FO_{0.5}$	1.10	0.60	500	800	500
					900

ΔM_{th}, expected weight loss; ΔM_{exp}, observed weight loss; T_{start}, beginning of CO_2 release; T_{end}, end of CO_2 release; $T_{Annealing}$, choice of annealing temperature; (*): from [18].

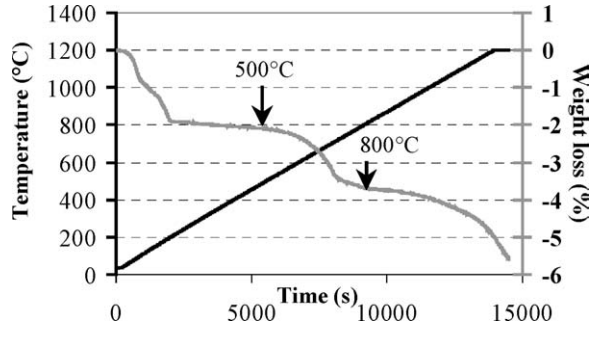

Figure 2 TGA of the reaction between "$Ca_7Nd_2(PO_4)_5(SiO_4)F$" (annealed at 1400°C for 6 h and 0.5 Cs_2CO_3).

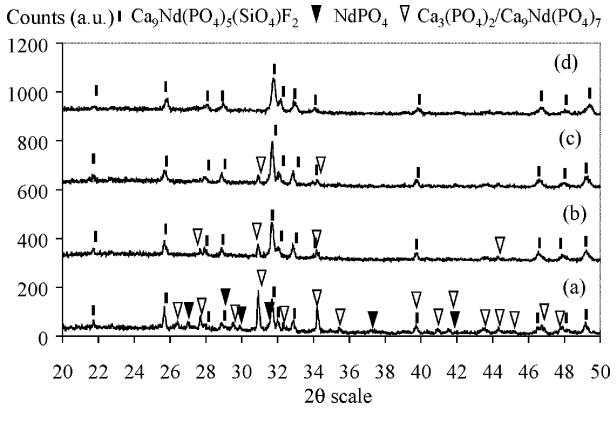

Figure 3 XRD patterns of $Ca_7Nd_2Cs(PO_4)_5SiO_4FO_{0.5}$: after Cs_2CO_3 addition, and further annealing at, 500°C for 1 h (a), 700°C for 1 h (b), 750°C for 1 h (c), 800°C for 1 h (d).

summarized in Table VI. Because they were poorly crystallized silica and cesium carbonate were not detected by this technique.

As it can be seen in Table VI, except for a Cs-bearing apatite containing 10 wt% of cesium annealed at 800°C (Fig. 3), the materials obtained were found to be multiphase. All the detected phases (except for Nd_3PO_7) had a molar ratio Me/X (Me = Ca or Ba + Nd + Cs; X = P + Si) equal to or below 1.667 which was the expected value for this parameter. With no evidence of additional weight losses on TG curves, this implied the presence of other phases with a Me/X ratio above 1.667. The reason why these phases were not identified could rely on their amorphous state or the overlapping of their reflections with those of the major phases. Another point was the fact that the localization of cesium (except for $CaCsNd(PO_4)_2$) was not clearly established from these results. Indeed, it was difficult to assess the concentration and phases which had incorporated this element.

The incorporation of cesium in apatites was expected to induce an increase of cell parameters due to a bigger ionic radius compared to calcium, neodymium or barium. But this was not observed in these experiments. It might be thus indicative of a weak trapped proportion and in order to further characterize these materials, a microanalysis by EDX was performed. Corresponding powders were pointed out in Table VI by a (♣) symbol. The data for $Ca_7Nd_2Cs(PO_4)_5(SiO_4)FO_{0.5}$ and $Ca_8NdCs(PO_4)_6FO_{0.5}$ were extracted from [18] and were obtained by an electron probe analysis. Corresponding compositions were pointed out in Table VI by a (•) symbol. These analyses are presented and discussed below (Table VII).

3.2.1. $Ca_7Nd_2Cs(PO_4)_5(SiO_4)FO_{0.5}$

The first phase was clearly assigned to the apatitic structure with a cesium content of 1.75 wt%. If this result was in agreement with the XRD analysis, the second phase, called "B", did not correspond to a defined compound. As it was not visible on XRD patterns, "B" was assumed to be partially amorphous.

3.2.2. $Ca_{8.10}Nd_{1.54}Cs_{0.36}(PO_4)_5(SiO_4)F_{1.82}O_{0.18}$

Three phases were found on the basis of EDX spectra: an apatite (1.85 wt% of cesium), a neodymium phosphate similar to Nd_3PO_7 and a $CaCsNd(PO_4)_2$-type structure with 26.56 wt% of cesium. This latter phase was not detected on XRD patterns and this should be explained by the overlapping of its main reflections ($2\theta = 28.861$ ($I/Io = 100$) and $2\theta = 31.612$ ($I/Io = 25$)) with those of the apatite. In addition, this effect could have been strengthened by a small proportion compared to the apatite. On the contrary, the monazite-type compound, $NdPO_4$, which was visible on the XRD patterns, was not identified due to the lack of grains belonging to this phase on the surface of the pellet.

TABLE VI Phases identification for the Cs-bearing apatites

Cs-bearing apatites/britholites	T (°C)	Phases detected by means of X-ray diffraction
1 "$Ca_7Nd_2Cs(PO_4)_5(SiO_4)FO_{0.5}$"	500	$Ca_9Nd(PO_4)_5(SiO_4)F_2$ (M); $Ca_9Nd(PO_4)_7$ (m); $NdPO_4$ (m).
	700	$Ca_9Nd(PO_4)_5(SiO_4)F_2$ (M); $Ca_9Nd(PO_4)_7$ (m); $NdPO_4$ (m).
	750	$Ca_9Nd(PO_4)_5(SiO_4)F_2$ (M); $Ca_9Nd(PO_4)_7$ (t); $NdPO_4$ (t).
	800•	$Ca_9Nd(PO_4)_5(SiO_4)F_2$ (M).
	820	$Ca_9Nd(PO_4)_5(SiO_4)F_2$ (M); $CsCaNd(PO_4)_2$ (m).
2 "$Ca_{8.10}Nd_{1.54}Cs_{0.36}(PO_4)_5(SiO_4)F_{1.82}O_{0.18}$"	500	$Ca_{10}(PO_4)_6F_2$ (M); Nd_3PO_7 (m); $NdPO_4$ (t).
	800♣	$Ca_{10}(PO_4)_6F_2$ (M); Nd_3PO_7 (m); $NdPO_4$ (t).
3 "$Ca_8NdCs(PO_4)_6FO_{0.5}$" (*)	770•	$Ca_{10}(PO_4)_6F_2$ (M); $Ca_3(PO_4)_2$ (m).
4 "$Ca_{9.18}Nd_{0.49}Cs_{0.33}(PO_4)_6F_{1.84}O_{0.16}$"	500	$Ca_{10}(PO_4)_6F_2$ (M); $Ca_3(PO_4)_2$ (t); $NdPO_4$ (t).
	800♣	$Ca_{10}(PO_4)_6F_2$ (M); $CaCsNd(PO_4)_2$ (t); $NdPO_4$ (t).
5 "$Ba_8NdCs(PO_4)_6FO_{0.5}$"	500	$Ba_{10}(PO_4)_6F_2$ (M), $Ba_3(PO_4)_2$ (M), $Ba_3Nd(PO_4)_3$ (M).
	900♣	$Ba_{10}(PO_4)_6F_2$ (M), $Ba_3(PO_4)_2$ (M), $Ba_3Nd(PO_4)_3$ (M).

M: major; m: minor; t: traces; (*): from [18];•: electron microprobe analysis performed; ♣: EDX microanalysis performed.

TABLE VII Compositions deduced from microanalysis (standard deviation is given in parenthesis for non calculated and/or non set values)

Cpd[1]	Phase	Ca (or Ba)	Nd	Cs	P	Si	O	F	O (Ch.)[2]	Cs wt (%)
1[3]	1	8.66	1.15	0.17	5.26	0.74	24.53	1.15	–	1.75
		(0.88)	(0.63)	(0.13)	(0.18)	(0.18)	(0.36)	(0.51)		
	2[4]	24.13	18.19	1.99	11.88	1.13	33.23	0.02	–	2.19
		(0.29)	(0.83)	(0.39)	(0.63)	(0.23)	(1.07)	(0.04)		
2	1	9.2	0.7	0.2	5.4	0.6	24	0.75	0.60	1.85
		(0.5)	(0.4)	(0.2)	(0.4)	(.4)				
	2	0.4	2.2	0.13	1.18	0.17	6.99	–	–	3.45
		(0.3)	(0.4)	(0.02)	(0.09)	(0.02)				
	3	1.25	0.8	0.96	1.78	0.3	7.99	–	–	26.52
		(0.03)	(0.1)	(0.01)	(0.08)	(0.2)				
3[3]	1	8.58	1.09	0.27	5.99	–	25.02	0.73	–	2.70
		(0.68)	(0.27)	(0.19)	(0.01)		(0.28)	(0.65)		
	2	2.56	0.43	0.10	1.99	–	7.98	–	–	3.31
		(0.10)	(0.06)	(0.05)	(0.00)		(0.01)			
4	1	9.87	0.10	0.03	5.83	0.17	24	0.75	0.58	0.03
		(0.03)	(0.02)	(0.02)	(0.17)	(0.07)				
	2	0.04	0.91	0.05	0.96	0.05	3.94	–	–	0.03
		(0.02)	(0.09)	(0.03)	(0.07)	(0.03)				
	3[5]	0.95	0.80	0.95	1.97	0.22	7.99	–	–	26.57
5	1[5]	2.97	0.89	0	3.08	–	12	–	–	0
	2[5]	2.66	0.04	0	2.11	–	8	–	–	0
	3	8.79	0.46	0.76	6	–	24	0.75	0.48	5.12
		(1.52)	(0.46)	(0.76)						
	4[5]	1.23	0	0.6	0.98	–	4	–	–	45.81
	5[5]	0.15	2.68	0.37	1.07	–	7	–	–	8.18

[1]: Cpd = Compound; this value refers to our notation for the different apatitic compounds as presented in Tables V or VI.
[2]: Ch = Channel; this value is calculated from the electric neutrality equation.
[3]: These results were reported in [18]. The materials were characterized by electron probe microanalysis and only a global value for the oxygen amount in the apatite is given.
[4]: Composition given with weight percents.
[5]: For these phases, only one measurement could be performed. No standard deviation is therefore indicated.

3.2.3. $Ca_8NdCs(PO_4)_6FO_{0.5}$

The first phase with a Me/X ratio equal to 1.667 was assigned to the apatite (2.70 wt% of cesium) and the second to a $Ca_3(PO_4)_2$-type phase. In spite of a global Me/X ratio less than 1.667 in this material, no other phase with Me/X > 1.667 was detected.

3.2.4. $Ca_{9.18}Nd_{0.49}Cs_{0.33}(PO_4)_6F_{1.84}O_{0.16}$

The three already identified phases were confirmed by this analysis. The presence of small amounts of silicon could have resulted from a contamination due to the polishing on SiC papers. Both the apatite and the monazite-type compound have incorporated less than 1 wt% of cesium. In this way, it was clearly shown that the element was preferentially immobilized in a $CaCsNd(PO_4)_2$-type phase. The proportion of which was moreover found to increase with annealing time.

3.2.5. $Ba_8NdCs(PO_4)_6FO_{0.5}$

Phases "1", "2" and "3", were already identified on XRD patterns. As usual, small cesium amounts were quantified into the apatitic form, "3". This element was found to be heterogeneously distributed within this compound as indicated by an important standard deviation. A particular Cs-bearing phase was also detected into agglomerates. As illustrated on Fig. 4a, the core of these agglomerates was made of small grains containing neodymium, phosphorus and oxygen (Fig. 4b). Their composition indicates a Nd_3PO_7-type compound. The Cs-bearing phase was located

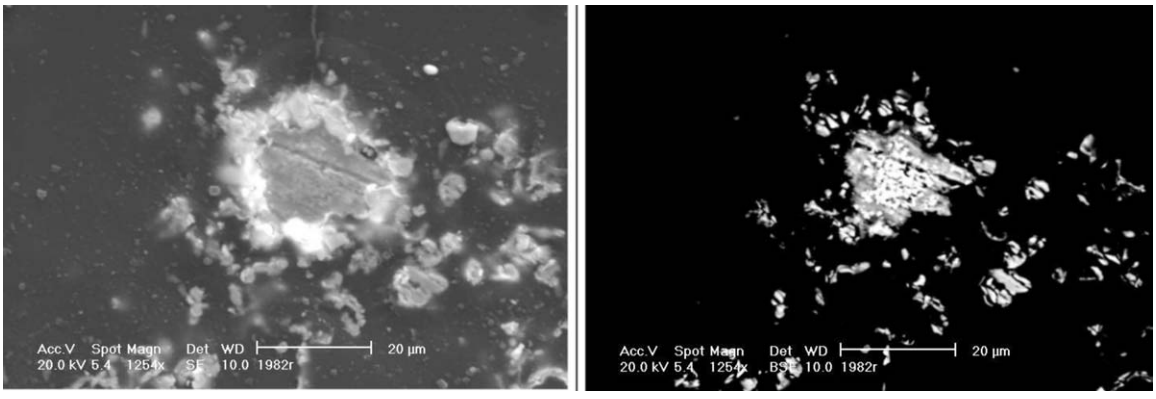

(a)

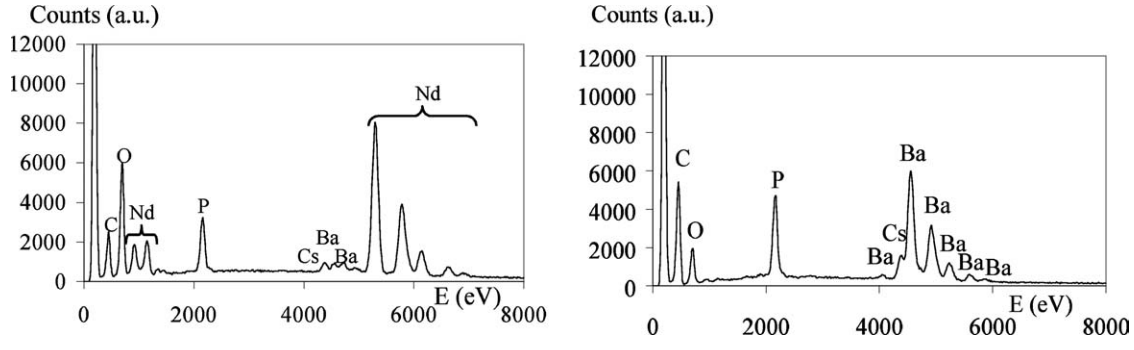

(b)

Figure 4 (a) SEM micrograph of Cs-bearing agglomerates in $Ba_8NdCs(PO_4)_6FO_{0.5}$: secondary electrons on the left side, backscattered electrons on the right side. (b) EDX spectra of Nd-bearing phase (left) and Cs-bearing phase (right) in $Ba_8NdCs(PO_4)_6FO_{0.5}$ agglomerates.

around this neodymium phosphate. Its general formula could not be correctly assessed because it was partially decomposed under the electronic beam. However, by comparison with other alkaline-alkaline earth phosphates with close molar ratio like $CaKPO_4$ [20], $SrKPO_4$ [21] or $Ca_2(K, Na)(PO_4)_2$ [22], its formula was assumed to be $BaCsPO_4$.

$BaCsPO_4$, as well as Nd_3PO_7, did not appear on XRD patterns and were probably amorphous.

Finally, whatever the composition which was considered, we found that cesium was effectively distributed among several compounds. Some, like $CaCsNd(PO_4)_2$, seemed to have a strong affinity for this element. Poorly crystallized compounds, like $BaCsPO_4$, with a similar property, were also detected.

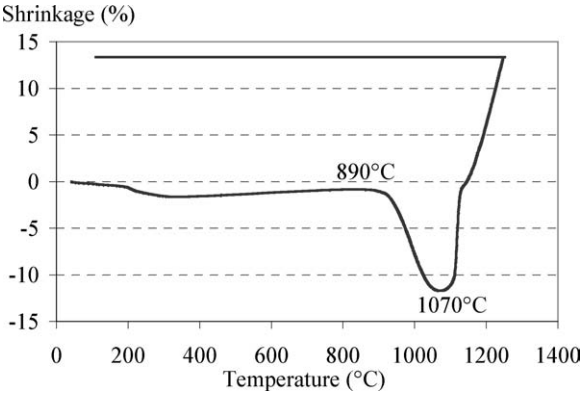

Figure 5 TMA of $Ca_7Nd_2Cs(PO_4)_5(SiO_4)FO_{0.5}$.

3.3. Densification behavior of $Ca_7Nd_2Cs(PO_4)_5(SiO_4)FO_{0.5}$ (10 wt% of cesium)

The initial material consisted of a powder annealed at 800°C for 1 h. This powder was ground in an attritor for 4 h in ethanol. Its surface then equaled 6.39 m^2/g. In order to determine the sintering temperature, the shrinkage of a pellet was followed by TMA (Fig. 5).

Two steps were identified. The first occurred between 890 and 1070°C with an inflection point at 993°C and the second, for temperatures above 1070°C, where a dramatic increase of the pellet height is observed. As weight losses due to a cesium release were observed above 1100°C, the second part of the shrinkage curve overlapped with the decomposition of the material.

In order to confine cesium during the sintering process, hot uniaxial pressing was performed under an argon flow. The ground powder was introduced in a cylindrical graphite matrix and boron nitride was used to isolate the pellet from the surface of the matrix and thus avoid carbon diffusion with temperature. Initial heating rate was set to 30°C/min. until a temperature of 900°C was reached. This temperature was then maintained for one hour before the material was allowed to cool. A pressure of 25 MPa was applied during the rise in temperature and the step at 900°C.

Final density, measured by He-pycnometry on a powder produced by grinding of a sintered pellet, was equal to 3.931 g/cm^3. Compared to a geometric measurement made on the sintered pellet prior to its grinding (3.822 g/cm^3), this led to a densification ratio of 97.2%.

As expected from the results gathered in Table VI, the sintering, which occurred for temperatures above 800°C, was reactive and resulted in the formation of a

TABLE VIII Composition of $Ca_7Nd_2Cs(PO_4)_5(SiO_4)FO_{0.5}$ (sintered pellet)

	Ca (%)	Nd (%)	Cs (%)	P (%)	Si (%)	F (%)
Theory	21.7	22.3	10.3	11.9	2.2	1.5
Analysis	21.1	17.8	11.1	11.4	1.4	0.9

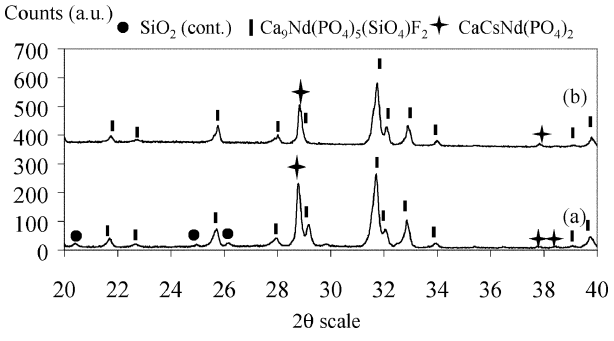

Figure 6 XRD patterns of $Ca_7Nd_2Cs(PO_4)_5(SiO_4)FO_{0.5}$ (sintered pellet) before (a) and after (b) the leach test procedure. SiO_2 came from a contamination during the polishing.

$CaCsNd(PO_4)_2$-type phase (Fig. 6a). Table VIII shows the theoretical composition for the pellet and that obtained by chemical analysis.

Except for neodymium, no significant difference, viz., greater than 1%, was observed. The anomalous behavior of neodymium still remains unclear.

3.4. Chemical durability evaluation of a material of theoretical composition $Ca_7Nd_2Cs(PO_4)_5(SiO_4)FO_{0.5}$

Starting material consisted of a sintered pellet as described in Section 3.3. Table IX shows the cesium release after 6, 14 and 30 days. After 1 day of experiment, this value is nearly the same as that after 6 days. This implied a dramatic release during the first 24 h (more than 75% of the initial amount). Therefore, this behavior was explained by the presence of quickly soluble phases containing cesium.

At the end of the test, the pellet was withdrawn and further characterized. This handling pointed out a severe exfoliation of the material.

TABLE IX Cesium release as a function of time during the leach test procedure for $Ca_7Nd_2Cs(PO_4)_5(SiO_4)FO_{0.5}$ (sintered pellet)

Time (d)	6	14	30
Amount of cesium dissolved (as a % of the solid content)	75.04	75.34	75.48

TABLE X Compositions deduced from the microanalysis (EDX) of $Ca_7Nd_2Cs(PO_4)_5(SiO_4)FO_{0.5}$ (sintered pellet) after the leach test procedure

Phase	Ca	Nd	Cs	P	Si	O	F	O (channel)	Cs (wt. %)
1	8.0 (0.3)	1.7 (0.4)	0.3 (0.1)	5.0 (0.3)	1.0 (0.3)	24	0.75	1.24	3.19
2	1.83 (0.07)	0.71 (0.04)	0.4 (0.1)	1.78 (0.05)	0.21 (0.02)	7.99	–	–	13.72

Standard deviation is given in parenthesis for non calculated and/or non set values.

The same two crystalline phases were identified by XRD before and after the leach test procedure (Fig. 6b). The first had the apatitic structure and the second was $CaCsNd(PO_4)_2$. As their relative proportion did not significantly seem to change, the general behavior of the pellet could not be explained by the dissolution of one of these two phases. Consequently, the Cs-rich quickly soluble phases were assumed to be poorly crystallized in the starting material. This observation was in agreement with the presence of an amorphous phase, B (see Section 3.2), in the powder before sintering.

To determine cesium distribution into the material, different samples were observed by SEM (Fig. 7) and their composition deduced from their EDX spectra. Table X summarizes the results obtained. Analyses on the same material (before the alteration) were impossible due to the grain size (less than 1 μm), smaller than the analyzed area, and the presence of soluble phases in grain boundaries. In this case no composition could be determined.

After being exposed to the leach test, a morphological change was clearly observed: grains were disconnected from the others (Fig. 7). This should be responsible for the macroscopic exfoliation of the pellet.

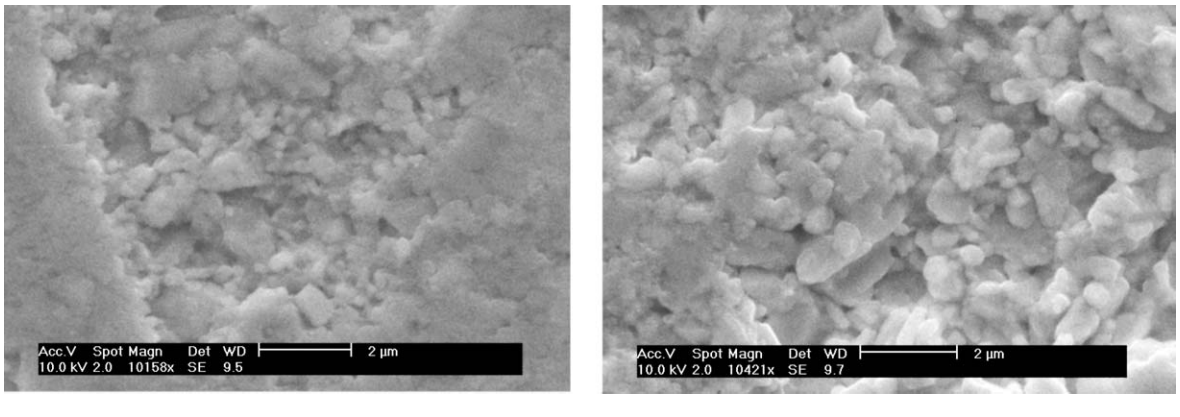

Figure 7 SEM micrograph of $Ca_7Nd_2Cs(PO_4)_5(SiO_4)FO_{0.5}$ before applying the leach test procedure (left) and after applying the leach test procedure (right).

The dissolution of a Cs-rich amorphous phase in grain boundaries was certainly the origin of the phenomenon. The analysis on isolated grains by EDX showed two different composition related to the two phases detected on XRD patterns. The $CaCsNd(PO_4)_2$-type phase, with 13.72 wt% of cesium, had a stronger affinity for cesium than the apatite (3.19 wt%).

4. Conclusion

Whatever the composition or annealing conditions, attempts to form a calcium/barium Cs-bearing apatite as a single phase were unsuccessful. Cesium was systematically found into at least one compound without the apatitic structure. Some, like $CsCaNd(PO_4)_2$, were quite sufficiently crystallized to be visible on XRD patterns but some, like $BaCsPO_4$, were mainly amorphous and sometimes highly soluble. Moreover, these phases had often incorporated significant amounts of cesium whereas weak contents, generally less than 3 wt%, were found for the apatite. Consequently, the aqueous durability of the bulk material, one of the most important criterion for cesium immobilization, greatly depended on the own durability of each phase. It was finally determined by the shortest lasting phase. Thus, the investigation of the durability of each by-product would be necessary. Such a study would not be realistic. Nevertheless, this work emphasizes the particular behavior of $CsCaNd(PO_4)_2$. The aqueous durability of this phosphate was unwittingly assessed during the leach test of the Cs-bearing ceramic with 10 wt% of cesium. In a detailed way, this test has underlined that $CsCaNd(PO_4)_2$ and the britholite were the only two crystalline phases to be visible on XRD patterns at the beginning and at the end of the procedure. Therefore, they seem to be water resistant and the presence of $CsCaNd(PO_4)_2$ do not seem to be a problem for the leaching behavior. In fact, litterature shows that $CsCaNd(PO_4)_2$ belongs to a large family of compounds able to incorporate the biggest alkaline cations like cesium or rubidium. They also exhibit a thermal stability higher than 900°C [23, 24]. From all the other results gathered in this work, the study of $CsCaNd(PO_4)_2$ as a possible cesium host could be of interest.

References

1. D. R. LIDE, "Handbook of Chemistry and Physics," 73rd ed. (CRC Press, Boca Raton, Florida, USA, 1992–1993), Section 11.
2. P. RENAUD, K. BEAUGELIN, H. MAUBERT and P. LEDENVIC, "Conséquences radiologiques et dosimétriques de l'accident de Tchernobyl en France" (Rapport IPSN 97-03, IPSN, France, 1997).
3. V. SERE, PhD thesis from University of Paris VII, France, 1996.
4. J. CARPENA and J. L. LACOUT, French Patent 08676 (1993).
5. J. CHAUMONT, S. SOULET, J. C. KRUPA and J. CARPENA, *J. Nucl. Mater.* **301**(2/3) (2002) 122.
6. H. McDOWELL, T. M. GREGORY and W. E. BROWN, *J. Res. Natn. Bur. Stand. A Phys. Sci.* **81A** (1977) 273.
7. J. C. ELIOTT, "Structure and Chemistry of the Apatites and Other Calcium Phosphates," Studies in Inorganic Chemistry 18 (Elsevier, Amsterdam, The Netherlands, 1994) p. 64.
8. J. CARPENA, F. AUDUBERT and J. L. LACOUT, French Patent 14706 (1994).
9. F. AUDUBERT, PhD Thesis from INP of Toulouse, France, 1995.
10. T. ROBIN, D. BERNACHE-ASSOLLANT and F. AUDUBERT, *J. Europ. Ceram. Soc.* **20** (1999) 1231.
11. T. ROBIN, PhD Thesis from University of Limoges, France, 2000.
12. L. BOYER, PhD Thesis from INP of Toulouse, France, 1998.
13. L. BOYER, J. CARPENA and J. L. LACOUT, *Solid State Ion.* **95**(1/2) (1997) 121.
14. M. MATHEW, W. E. BROWN, M. AUSTIN and T. NEGAS, *J. Solid State Chem.* **35** (1980) 69.
15. C. VIGNOLES, PhD Thesis from University of Toulouse III, France, 1973.
16. G. BONEL, J. C. LABARTHE and C. VIGNOLES, in Proceedings of Colloques Internationaux du Centre National de la Recherche Scientifique, Physico-Chimie et Cristallographie d'Intérêt Biologique, Paris, 1973, edited by CNRS (Paris, 1975) Vol. 230, p. 117.
17. N. SENAMAUD, D. BERNACHE-ASSOLLANT, J. CARPENA and C. PIN, *Mat. Res. Soc. Symp. Proc.* **556** (1999) 93.
18. N. SENAMAUD, PhD Thesis from University of Limoges, France, 1999.
19. French AFNOR draft standard X 30-403.
20. M. A. BREDIG, *J. Phys. Chem.* **46** (1942) 747.
21. L. EL AMMARI, M. EL KOUMIRI, W. DEPMEIER, K. F. HESSSE and B. ELOUADI, *Eur. J. Solid State Inorg. Chem.* **34** (1997) 563.
22. N. JINLONG, Z. ZHENXI, J. DAZONG, Y. SHENGHONG, M. GUANGLAI and W. KEGUANG, *J. Mater. Sci.* **36** (2001) 3805.
23. M. ET-TABIROU and A. DAOUDI, *C.R. Acad. Sci. Paris, Ser.* C **291** (1980) 93.
24. L. P. KELLER, G. J. McCARTHY and R. G. GARVEY, *Mat. Res. Bull.* **20** (1985) 459.

Received 15 April 2003
and accepted 27 April 2004